Risley Scanner using a Metasurface Source and a Single Deflector for SATCOM Applications

M. Bertrand, J. Ruiz-Garcia, J.-F. Allaeys, D. Gonzalez-Ovejero, T. Q. V. Hoang, B. Loiseaux, Ronan Sauleau, R. Czarny, Mauro Ettorre

▶ **To cite this version:**

M. Bertrand, J. Ruiz-Garcia, J.-F. Allaeys, D. Gonzalez-Ovejero, T. Q. V. Hoang, et al.. Risley Scanner using a Metasurface Source and a Single Deflector for SATCOM Applications. IEEE Transactions on Antennas and Propagation, 2024, 72 (6), pp.4839 - 4851. 10.1109/tap.2024.3395908 . hal-04596451

HAL Id: hal-04596451
https://hal.science/hal-04596451

Submitted on 2 Jul 2024

HAL is a multi-disciplinary open access archive for the deposit and dissemination of scientific research documents, whether they are published or not. The documents may come from teaching and research institutions in France or abroad, or from public or private research centers.

L'archive ouverte pluridisciplinaire **HAL**, est destinée au dépôt et à la diffusion de documents scientifiques de niveau recherche, publiés ou non, émanant des établissements d'enseignement et de recherche français ou étrangers, des laboratoires publics ou privés.

Distributed under a Creative Commons Attribution - NonCommercial 4.0 International License

This article has been accepted for publication in IEEE Transactions on Antennas and Propagation. This is the author's version which has not been fully edited and content may change prior to final publication. Citation information: DOI 10.1109/TAP.2024.3395908

Risley Scanner using a Metasurface Source and a Single Deflector for SATCOM Applications

M. Bertrand, J. Ruiz-García, *Member, IEEE*, J.-F. Allaeys, D. González Ovejero, *Senior Member, IEEE*, T. Q. V. Hoang, B. Loiseaux, R. Sauleau, *Fellow, IEEE*, R. Czarny, and M. Ettorre, *Fellow IEEE*

***Abstract*—This paper presents a 2D-beam-steering antenna for Satcom applications based on a simplified Risley scanner, which consists of a leaky-wave feed and a single deflector fabricated by additive manufacturing. Such a configuration simplifies classical Risley scanners, where a source illuminates a combination of two prisms. The pointing direction of the radiated beam is controlled by the relative azimuthal positions between the leaky-wave feed and the deflector. The leaky-wave feed comprises a modulated metasurface antenna fed by a quasi-optical system to maximize its aperture efficiency. The angular dispersion of the metasurface is engineered to reduce the beam squint in the frequency band of interest while preserving the efficiency and compactness of the structure. In turn, the deflector is composed of partially dielectric-loaded metallic waveguides, achieved through the combination of two additively manufactured parts. A prototype validates the concept showing a field of view of 360° in azimuth and 50° in elevation with a maximum realized gain of 25.4 dBi at broadside at 20.2 GHz.**

***Index Terms*—Additive manufacturing, metasurfaces, PCB, Risley scanner, SATCOM, terminal antennas, wide-angle steering.**

I. Introduction

SATELLITE communications using Low Earth Orbit (LEO) constellations are attracting a strong interest for their capability to provide fast data connections worldwide [1]. However, the promised data rate and low latency of LEO communications require user terminals with highly directive beams and a large field-of-view to establish resilient links with fast-moving LEO satellites. In addition, user terminals should satisfy stringent requirements in terms of compactness, cost and energy consumption to fulfill the needs of the mass market. In this context, different beam-steering mechanisms are competing to address the demands of Satcom terminals, namely mechanical, electronic and hybrid steering [1]. Electronically-steered antennas such as phased arrays are the most agile solutions, and current activities aim at reducing their cost, complexity and power consumption [2], [3].

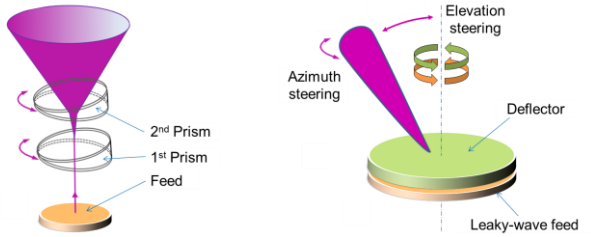

(a) (b)

Fig. 1. Risley scanner. (a) Classical implementation. (b) Proposed architecture.

Mechanical beam-steering antennas, on the other hand, can allow very effective solutions, even low profile, with minimal movements [4]-[9]. In the context of mechanically steered antennas, this paper focuses on the Risley scanner [10], [11]. Such an architecture has the advantage of achieving a wide field of view without complex mechanical platforms. Fig. 1(a) shows the classical architecture of a Risley scanner. It consists of a feed and two prisms. These elements are aligned with the main axis of the scanner. The feed illuminates the prisms with a beam parallel to the axis of the scanner. The azimuthal positions of the prisms control the pointing direction of the radiated beam in azimuth and elevation [10], [11]. Although very effective, this solution is very cumbersome in its classical implementation with dielectric wedges, as shown in Fig. 1(a).

To address this limitation, recent works have mainly focused on two alternative solutions. The first solution consists in using low-profile directive feeds realized by printed circuit board (PCB) technology, such as radial-line slot arrays or metasurface antennas [12], [13]. This way, one reduces the distance between the source and the first prism and, at the same time, the profile of the source. The second solution replaces the bulky refracting prisms by low-profile deflectors, with either metallic patterns [12]-[16] or all-dielectric solutions [17], [18]. These approaches rely on two rotating components to control the beam pointing direction.

Recently, the new architecture shown in Fig. 1(b) has been proposed to further reduce the profile of the whole structure [19]. In that case, the first rotating prism and the feed in the

Manuscript received May XX, 2023; accepted XXX XX, 20XX. Date of publication XXX XX, 20XX; date of current version XXX XX, 20XX. This work was supported by ANR under Grant ANR-17-ASTR-0010.

M. Bertrand, J.-F. Allaeys, T. Q. V. Hoang, B. Loiseaux and R. Czarny are with Thales Group, France.

D. Gonzalez-Ovejero and R. Sauleau are with Université de Rennes, CNRS, IETR, Rennes, France.

At the time of this work J. Ruiz-García and M. Ettorre were with the Université de Rennes, CNRS, IETR, Rennes, France.

J. Ruiz-García is with the Electrical Engineering and Computer Science Department, University of Michigan, Ann Arbor, MI 48109 USA.

Mauro Ettorre is currently with the Electrical and Computer Engineering Department, Michigan State University, East Lansing, MI 48824 USA (ettorre@msu.edu).

ACCEPTED MANUSCRIPT / CLEAN COPY

This article has been accepted for publication in IEEE Transactions on Antennas and Propagation. This is the author's version which has not been fully edited and content may change prior to final publication. Citation information: DOI 10.1109/TAP.2024.3395908

classical Risley configuration are replaced by a rotating leaky-wave feed. The leaky-wave feed is based on a metasurface antenna and generates a tilted beam to illuminate a single prism. The prism is made of a discrete lens based on a phase-shifting surface (PSS). The relative azimuthal positions of the prism and the leaky-wave feed around the main rotation axis of the scanner control the beam pointing direction in elevation and azimuth as in classical Risley scanners. A field-of-view of 360° in azimuth and ±57° in elevation is reported at 10 GHz. The main advantage of the proposed architecture is the very low profile of about 1.1 free space wavelength at 10 GHz. However, the frequency dispersion of the leaky-wave feed may impact the field-of-view of the scanner and its instantaneous bandwidth for Satcom links. In other words, in classical Risley scanners the pointing direction of the radiated beam is only controlled by the azimuthal positions of the prisms. In [19], frequency also has an effect on the pointing direction of the radiated beam due to the frequency scanning behavior of the leaky-wave feed. In addition, a tradeoff between aperture efficiency / bandwidth / frequency dispersion should be found for the leaky-wave feed to provide a reasonable instantaneous bandwidth of the radiated beam for high data-rate links [1]. Instantaneous bandwidths of hundreds of MHz are required for Gb/s communications for Satcom applications.

In this work, the simplified architecture shown in Fig. 1(b) is adopted to propose a novel Risley scanner, as shown in Fig. 2. It consists of a leaky-wave feed and a single deflector based on additive manufacturing.

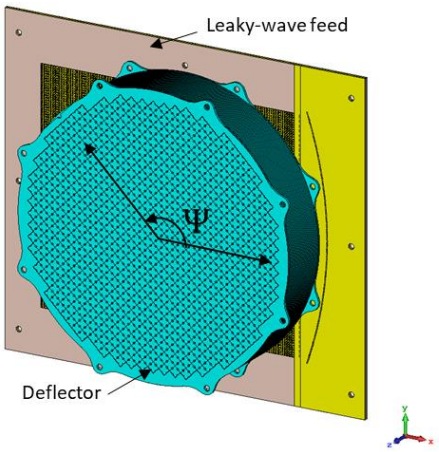

Fig. 2. Perspective view of the proposed Risley scanner. The angular orientation Ψ between the leaky-wave feed and the deflector controls the angle between the radiated beam and the antenna normal.

Preliminary results for this architecture were presented in [20]. The leaky-wave feed comprises a linearly polarized metasurface [21], [22], fed by an integrated pillbox quasi-optical beam-former [23]-[26]. The metasurface is engineered to minimize the frequency dispersion of the radiated beam and achieves an aperture efficiency exceeding 50% over the 19.2-21.2 GHz band. The main pointing direction of the metasurface is chosen equal to -32° in elevation at the central frequency of 20.2 GHz to allow a field of view of about 60° in elevation with the Risley scanner. A quasi-optical system based on a pillbox transition is adopted to illuminate the metasurface, which may pave the way for multiple beam radiations for resilient Satcom links [1].

The deflector combines two additively manufactured and complementary parts, namely an array of quad-ridged waveguides in Titanium, and a dielectric filling in Acrylonitrile Butadiene Styrene (ABS). This configuration leverages the potential of a hybrid deflector implementation, as an alternative to fully dielectric solutions [27]. The waveguides define in the targeted band a square lattice of $\lambda_0/2$ periodicity (with λ_0 being the wavelength in free space at the central frequency). This choice limits the impact of grating lobes, while providing sufficient phase excursion with a reduced frequency dispersion. The final 49-mm-thick deflector provides 270° phase excursion with only 5° of dispersion within the 19.2-21.2 GHz frequency band. The spacing between the leaky-wave feed and the deflector has been also optimized to reduce reflections for both Transverse Electric (TE) and Transverse Magnetic (TM) polarizations.

The final size of the Risley scanner (comprising deflector and leaky-wave feed) is about 250 mm of diameter with a total thickness lower than 65 mm. Measurements demonstrate the capability of the system to cover a field of view of 360° in azimuth and 50° in elevation in the 19.2-21.2 GHz band with a maximum measured gain exceeding 25 dBi at 20.2 GHz.

The paper is organized as follows. Section II presents the leaky-wave feed. The deflector is presented in Section III with a focus on the selection of the waveguide geometry and matching. The prototype and measurements are presented in Section IV. Finally, conclusions are drawn in Section V.

II. Leaky-Wave Feed

The leaky-wave feed (LWF) combines a pillbox quasi-optical beam-former [23]-[26] and a sinusoidally modulated metasurface (MTS) [21], [22], which results in a compact, highly efficient feed. Fig. 3 shows a perspective view of the LWF, which consists of two stacked parallel plate waveguides (PPWs) accommodating the pillbox transition and the modulated metasurface. The pillbox transition connects both PPWs using a 180° bend with a parabolic profile. As a result, the pillbox transforms a transverse electromagnetic (TEM) cylindrical wavefront launched by a primary feed in the bottom PPW (bottom part in Fig. 3) into a planar one in the top substrate to illuminate the metasurface. A slotted transition (insets in Fig. 3) ensures a smooth conversion between the TEM mode in the top PPW and the TM (transverse magnetic) surface wave mode bounded to the metasurface. In the proposed LWF, the pillbox has a focal distance $F_d = 15.1$ cm, and a diameter $D_d = 21$ cm. The dimensions of the primary feed, showcased in Fig. 3, are $w = 8.5$ mm, $w_a = 20$ mm, $L_{wg} = 3$ mm and $L_{horn} = 20$ mm. The pillbox-based feeding approach provides high feeding efficiencies of the MTS, comparable to other excitation mechanisms such as coaxial feeds [28], [29]. In addition, it allows the integration of several primary sources in the pillbox focal plane providing a multi-beam capability for the final system [23]-[25]. It has been shown that modulated MTSs enables the introduction of complex radiative functionalities

ACCEPTED MANUSCRIPT / CLEAN COPY

This article has been accepted for publication in IEEE Transactions on Antennas and Propagation. This is the author's version which has not been fully edited and content may change prior to final publication. Citation information: DOI 10.1109/TAP.2024.3395908

[30], [31].

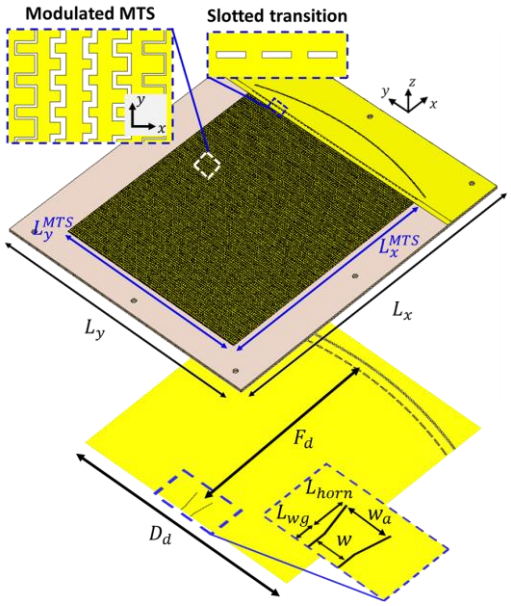

Fig. 3. Perspective view of the proposed leaky-wave feed. The pillbox layout is represented at the bottom. Insets show the modulated MTS, the slotted transition from the pillbox to the MTS and details of the primary feed.

In our case, the MTS plays a double role: it generates a directive beam at a desired pointing angle and it minimizes the frequency dispersion of the LWF, which ensures a high stability of the beam over the frequency band of interest. This novel functionality is detailed in the following.

A. Dispersion Analysis of the Metasurface

We aim to reduce the frequency scanning of the beam radiated by the LWF. To this end, we need to find the design parameters of the MTS that minimize the frequency dispersion. The MTS is treated as a modulated capacitive sheet (penetrable) impedance $Z_s = jX_s$ [30], [32], [33], with $X_s < 0$ and a spatial modulation given by:

$$Z_s(x) = jX_{s,av}\left[1 + M\cos\left(\frac{2\pi x}{p}\right)\right]. \quad (1)$$

The design parameters include: the design frequency f_d, the average sheet reactance $X_{s,av}$, the modulation depth M, the modulation period p, and the thickness d_{sub} and relative permittivity ε_r of the substrate. Furthermore, the combined effect of the capacitive sheet impedance and the grounded dielectric yields an equivalent inductive opaque (impenetrable) impedance $Z_{op} = jX_{op}$, with $X_{op} > 0$ [22], [30], [32].

Given the periodicity of Z_s in (1), the total field can be expressed as a sum of Floquet harmonics. The aforementioned design parameters can be tailored so only the $n = -1$ harmonic enters in the visible region. Thus, the surface wave is gradually transformed into a LW and a directive beam is radiated. It is possible to analytically estimate the elevation pointing angle θ_0 of the radiated beam at a given operation frequency f as in [22], [23]. Then, we can study the variation of θ_0 within the frequency band of interest for different combinations of the MTS' design parameters. For the angular dispersion analysis, we set $f_d = 20.2$ GHz and $M = 0.3$. For a given value of the average opaque reactance $X_{op,av}$ (or average sheet reactance $X_{s,av}$), M, ε_r and d_{sub}, the modulation period p can be tuned to obtain a desired θ_0 using:

$$\sin\theta_0 = \frac{k_x}{k_0} - \frac{2\pi}{pk_0}. \quad (2)$$

In (2), k_x corresponds to the transverse wavenumber of the fundamental Floquet mode ($n = 0$), obtained from solving the dispersion problem for modulated sheet impedances [21]. In the presented parametric study, p is adjusted to maintain $\theta_0 = -32^o$ at 20.2 GHz for each combination of $X_{op,av}$, ε_r and d_{sub}. Fig. 4(a) shows the variation of θ_0, defined as $\Delta\theta_0$,within the 19.2 – 21.2 GHz band for different values of $X_{op,av}$ and ε_r with $d_{sub} = 1$ mm. We use $X_{op,av}$ in this analysis just as an input parameter and to simplify the data representation in Fig. 4. For each combination of $X_{op,av}$, ε_r and d_{sub}, the resulting $X_{s,av}$ is computed and used to estimate $\Delta\theta_0$. As observed, the angular dispersion decreases for smaller ε_r, whereas the variation of $X_{op,av}$, or its equivalent $X_{s,av}$, has a minor impact. We also verified that $\Delta\theta_0$ is practically independent of d_{sub}, as represented in Fig. 4(b). In these figures, η_0 corresponds to the free-space wave impedance. The missing portions in Fig. 4(a)-(b) correspond to combinations of modulation parameters that do not produce a radiated beam at some frequencies in the band of interest. Specifically, such modulation parameters result in an imaginary value of θ_0 in (2) ($|\sin\theta_0| > 1$). Finally, the variation of the half-power beamwidth (HPBW) is also studied and proved to be stable over the bandwidth, as shown in Fig. 4(c) for $\varepsilon_r = 2.2$ and $d_{sub} = 1.575$ mm. For the latter values of ε_r and d_{sub}, the estimated angular dispersion within the frequency band of interest is plotted in Fig. 4(d), yielding $\Delta\theta_0 = 14.3^o$.

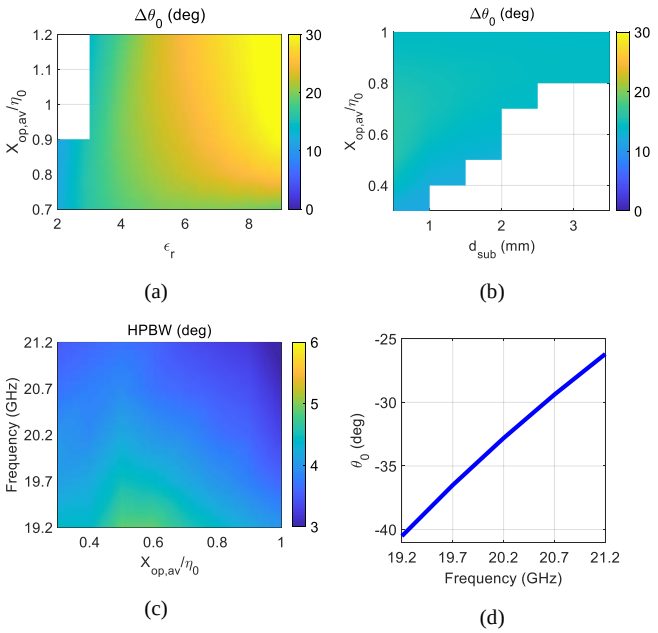

Fig. 4. (a) Variation of beam direction $\Delta\theta_0$ of the LWF for different values of ε_r and $X_{op,av}$, fixing $d_{sub} = 1$ mm. (b) Values of $\Delta\theta_0$ obtained for different values of d_{sub} and $X_{op,av}$, fixing $\varepsilon_r = 2.2$. (c) Change in HPBW within the frequency band of interest for different values of $X_{op,av}$, fixing

ACCEPTED MANUSCRIPT / CLEAN COPY

This article has been accepted for publication in IEEE Transactions on Antennas and Propagation. This is the author's version which has not been fully edited and content may change prior to final publication. Citation information: DOI 10.1109/TAP.2024.3395908

$\varepsilon_r = 2.2$ and $d_{sub} = 1.575$ mm. (d) Pointing direction vs. frequency for the final LWF.

Considering the available commercial substrates, we finally adopt a Rogers RT5880 substrate with $\varepsilon_r = 2.2$, $d_{sub} = 1.575$ mm and $\tan\delta = 0.0009$. Hence, the stack-up of the pillbox system and MTS (Fig. 3) is made by two Rogers RT5880 substrates glued by a 78-μm thick bonding layer (Taconic fastRise™ FR-27-0030-25, with relative permittivity of 2.7 and $\tan\delta = 0.0017$). The chosen thickness ensures the mechanical robustness of the system. As presented in the next subsection, the MTS is designed to radiate a beam at $\theta_0 = -32^o$ at $f_0 = 20.2$ GHz. The goal is to compensate the deflection angle of the deflector to point at broadside when LWF and deflector are aligned. The deflector is described in Section III.

B. *Design of the Quasi-optically Fed Metasurface*

The unit cell used to implement the modulated MTS is presented in Fig. 5; it includes a meander slot etched on the top metallization of a grounded dielectric slab. The sub-wavelength cell has a dimension $a = 2$ mm ($a \approx \lambda_0/7.4$). The meander slot geometry is characterized by its width g, and arms' lengths l_1 and l_2 (see inset in Fig. 5(b)).

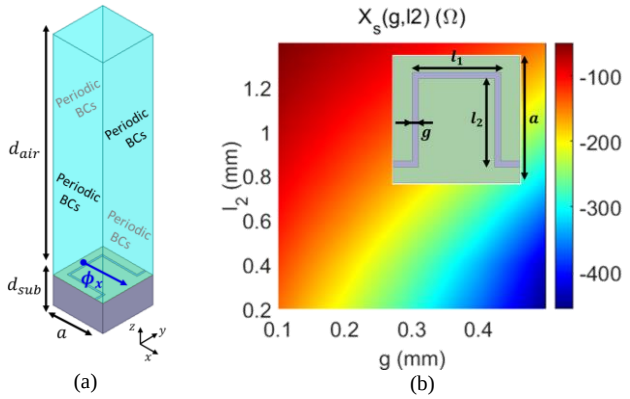

(a) (b)

Fig. 5. (a) Unit cell set-up for extracting effective Z_s ($d_{sub} = 1.575$ mm, $a = 2$ mm, $d_{air} = 12a$); periodic boundary conditions are set on the lateral walls. (b) Effective local X_s as a function of g and l_2 at f_0; the inset shows a top view of the unit cell with the geometrical parameters.

In order to synthesize the spatially-varying sheet impedance in (1), a database is generated to relate different combinations of g, l_1 and l_2 with the effective local sheet impedance Z_s. We use a full-wave simulator (Ansys HFSS) to build the cell set-up in Fig. 5(a). Periodic boundary conditions are imposed on the lateral boundaries of the airbox and the substrate. For a fixed $l_1 = 1.4$ mm, we use the eigenmode solver of HFSS to find the phase delay ϕ_x at $f_d = 20.2$ GHz for different combinations of g and l_2. Next, the effective sheet impedance can be computed [32]. Fig. 5(b) shows the effective local sheet reactance at f_d for different values of g and l_2. After building the impedance database, the modulated MTS is implemented. As already mentioned, the generated linearly-polarized beam is intended to point at $\theta_0 = -32^o$ at f_0. However, when the MTS is mounted on the pillbox beamformer, the evolution of the modulation, as well as the direction of the illuminating plane wave, is along $-\hat{x}$. Therefore, referring to the coordinate system of the LWF structure in Fig. 3, the generated beam will point at $\theta_0 = 32^o$ at f_0. The modulation was designed so that the surface wave power reaching the edge of the structure is smaller than -15 dB with respect to the illuminating mode to reduce edge effects. This is achieved by properly imposing the required leakage factor α, which is mostly defined by $X_{s,av}$ and M [21], [22]. For a total length along the x-axis of $L_x^{MTS} = 15.1\lambda_0$ (22.4 cm), the design parameters of the modulated MTS are $X_{s,av} = -170.9\,\Omega$ ($X_{op,av}/\eta_0 = 0.65$), $M = 0.7$, and $p = 8.43$ mm. The MTS width along the y-axis is $L_y^{MTS} = 13.7\lambda_0$ (20.4 cm). The resulting spatially-modulated sheet reactance $X_s(x)$ is plotted in Fig. 6 (blue line). Next, the required reactance value at each unit cell is mapped to the corresponding unit-cell geometry through the database in Fig. 5(b). As a result, we obtain the spatially-varying geometrical parameters $g(x)$ (dashed red line) and $l_2(x)$ (solid red line) represented in Fig. 6. The final lateral dimensions of the leaky-wave feed, including pillbox transition and MTS (see Fig. 3), are L_x=32.6 cm ($21.9\lambda_0$) and L_y=28.5 cm ($19.3\lambda_0$) with a total thickness thinner than 3.3 mm ($0.22\lambda_0$).

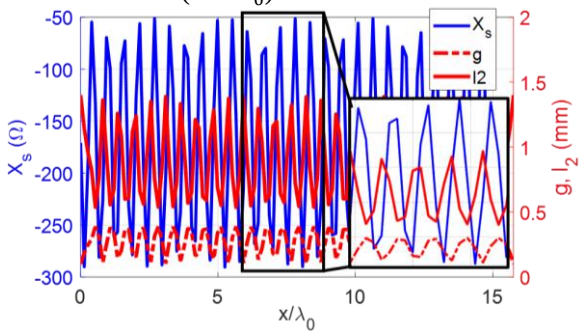

Fig. 6. Spatial variation of X_s (blue line), g (dashed red line) and l_2 (solid red line).

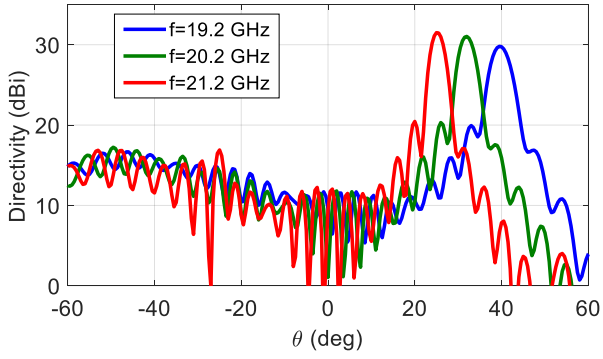

(a)

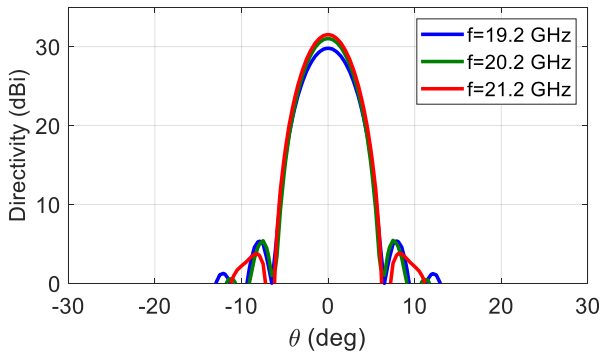

(b)

ACCEPTED MANUSCRIPT / CLEAN COPY

This article has been accepted for publication in IEEE Transactions on Antennas and Propagation. This is the author's version which has not been fully edited and content may change prior to final publication. Citation information: DOI 10.1109/TAP.2024.3395908

Fig. 7. Simulated directivity patterns of the LWF in the frequency band of operation in the (a) E-plane and (b) H-plane.

Fig. 7 shows the simulated radiation patterns in the E- and H-plane of the structure in Fig. 3. The edge taper of the pillbox system shapes the aperture field along the H-plane, whereas the modulated MTS controls the E-plane. As expected, the simulated elevation pointing angle of the LWF changes $\Delta\theta_0 = 14.2^o$ in the frequency band of operation, with $\theta_0 = 32^o$ at 20.2 GHz. A simulated aperture efficiency exceeding 52% over the entire frequency band of interest is obtained, as shown in Fig. 8. Furthermore, the simulated reflection coefficient stays below -20 dB over the entire frequency band (Fig. 8).

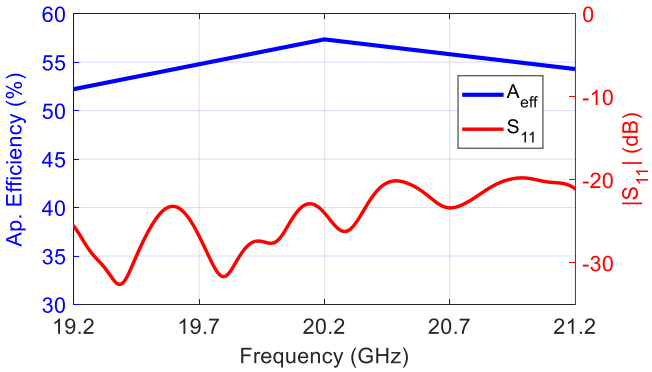

Fig. 8. Simulated aperture efficiency (blue line) and $|S_{11}|$ (red line) of the LWF in the frequency band of operation.

III. Deflector

The hybrid deflector structure is made of collinear metallic waveguides loaded with a specific amount of dielectric material to implement a phase gradient. The waveguides are designed to fit within a square grid with 7-mm pitch to remove grating lobes produced by the regular lattice up to 21.2 GHz. A minimum wall thickness of 0.5 mm has to be taken into account for fabrication constraints. It can be readily shown that with such square waveguides, the frequencies of interest lie below the cut-off frequency. To solve this problem, two methods were investigated. The first one considered loaded square waveguides to lower the cut-off frequency. The second one consisted in modifying the geometry of the transverse section of the waveguide with the addition of metallic ridges. These two approaches led to the selection of a suitable quad-ridged waveguide geometry which is presented below.

It is important to point out that the implementation of an arbitrary deflection with good efficiency generally requires at least a 360° range of variation of the transmission coefficient phase. However, given a limited waveguide length and cross section area, such a wide phase range can be challenging to obtain. Obviously, the phase range also depends on the relative permittivity ε_r of the dielectric material loading the waveguide. In this work, we decided to limit our investigation to the well-known ABS polymer. While its relative permittivity is relatively low ($\varepsilon_r = 2.56, tan\delta = 0.005$), it is a commercially available dielectric material being easily printable by standard Fused-Deposition Modeling (FDM) process with high repeatability and sufficient resolution. Therefore, the use of a phase range smaller than 360° was considered to achieve the deflection function with a reasonable waveguide length.

TABLE I
Simulated Characteristics of the Considered Waveguides

Waveguide	SW	QRSW
Frequency band (GHz)	19.2 – 21.2	19.2 – 21.2
***L* (mm)**	45	45
$\Delta\varphi$ (°)	283	281
$d\Delta\varphi$ (°)	49	5

A. Loaded waveguide analysis

In order to define the waveguide geometry for the deflector, various configurations with various transverse shapes and lengths were analyzed using a Floquet mode excitation in a periodic environment and evaluated based on three criteria.

The primary criterion for the comparison between these configurations is the achievable transmission phase variation $\Delta\varphi$ between minimal and maximal dielectric filling factors. In particular, for each geometry, the maximal dielectric filling is set by allowing at least 0.5 mm gap between the dielectric loading and the waveguide metallic walls. This margin was found empirically to enable an easy assembly.

The second criterion considered the frequency dispersion of the phase range $\Delta\varphi$, denoted $d\Delta\varphi$ and defined as the maximum deviation of the phase excursion in the analyzed frequency band. Such a dispersive behavior results in a variation of the synthetized phase distribution on the deflector aperture when varying the frequency. This variation should be avoided, in particular when 360° phase wrappings are placed at specific locations to deal with a limited available phase range. Such a variation leads to misplaced phase wrapping, causing degraded efficiency. In the case of a diffractive component based on a spatially periodic phase distribution as implemented here, such a variation may also lead to an increase of unwanted diffraction orders amplitudes.

The last criterion aimed at keeping as short as possible the required waveguide to reduce the deflector thickness. Based on these considerations, several waveguide geometries were numerically analyzed to achieve a trade-off between operating frequency band, waveguide length and phase dispersion. In the following, we will present two selected geometries and compare their performance based on the introduced criteria.

1) Square waveguide

The geometry of a square waveguide (SW) with inner dimension a= 6.5 mm is shown in Fig. 9. The dielectric filling is defined in the cross-section by the parameter $\tau_{SW} = \delta/a$, which is limited to $\tau_{SW}^{max} = 0.86$, leaving a 0.5 mm margin on each side.

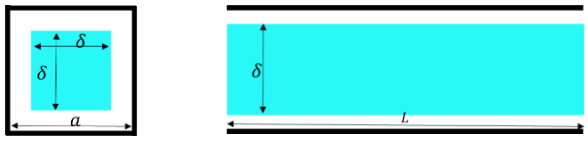

(a) (b)

Fig. 9. Geometry of the square waveguide (SW). (a) Transverse section. (b) Longitudinal section. The blue square represents the dielectric loading the waveguide.

ACCEPTED MANUSCRIPT / CLEAN COPY

This article has been accepted for publication in IEEE Transactions on Antennas and Propagation. This is the author's version which has not been fully edited and content may change prior to final publication. Citation information: DOI 10.1109/TAP.2024.3395908

2) Quad-ridged waveguide

The geometry of the proposed quad-ridged square waveguide (QRSW) is shown in Fig. 10. The dimensions of the QRSW are $a_1 = 6.5\,mm$, $b_1 = 3.9\,mm$, $c_1 = 2.5\,mm$, with wall and ridges thickness of 0.5 mm.

As the metallic ridges restrict the available space for the dielectric part, we opted for a variant filling along the length of the waveguides, less prone to printing tolerances. Thus, it is defined as $\tau_{QRSW} = L'/(L_0 + L/2)$, where L' defines the penetration depth of identical ABS tips inside the two opposite sides of the waveguide as shown in Fig. 10 (b), L' ranges from 0 to $L_0 + L/2$, so that the maximum filling ratio reaches $\tau_{QRSW}^{max} = 1$. The dielectric tip for progressive filling is fixed to $L_0 =$ 15 mm and $\delta_1 = 2.79$ mm, which corresponds to 10 printed layer thickness's and leaves a margin close to 1 mm with the metallic part for easier mounting. Finally, a supporting dielectric layer of thickness $L_m = 2\,mm$ was added at the external interfaces, and the ridges were slightly slanted to improve matching to free space.

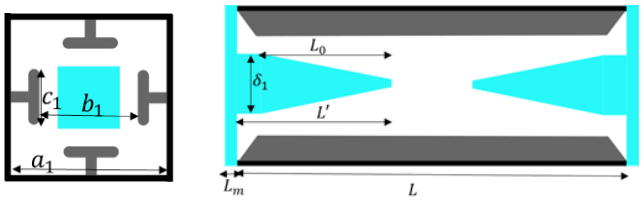

(a) (b)

Fig. 10. Geometry of the quad-ridged square waveguide (QRSW). (a) Transverse section. (b) Longitudinal section.

3) Performance comparison

The phase variation obtained under Floquet mode excitation at normal incidence for the SW and the QRSW are depicted in Fig. 11 (a) and (b), respectively. For each case, the phase variation is normalized to the phase obtained with the largest filling factor. The comparison between the waveguides is given in Table I. The SW, although being very simple, presents a strong dispersion due to the proximity of the cut-off frequency of the waveguide when using the smallest dielectric filling. It can be seen by the large variation of the phase obtained with the lowest filling factor of 0.66. One can achieve a 283° phase variation with a filling factor in the range of 0.66-0.86 with 45 mm length in the frequency band of 19.2-21.2 GHz. However, the dispersion reaches 49° in this band since the cut-off frequency is close to 17.8 GHz. Larger phase ranges could be obtained at the cost of longer waveguides and larger dispersion. The use of metallic ridges inside the waveguides shifts the cut-off frequencies downward even without dielectric filling, thus strongly reducing the dispersive behavior of the waveguides. As a result, the QRSW can provide 281° of phase variation with a dispersion as low as 5^o between 19.2 and 21.2 GHz.

B. Deflector synthesis

Based on the previous analysis, we selected the QRSW for implementing the deflection function with a 45 mm thickness and a small dispersion of the phase profile. Let us consider a deflector having $\hat{\boldsymbol{z}}$ as a normal, and achieving deflection in the xz-plane by an angle θ_{def} from the normal. A conventional starting point for implementing the deflection function is an aperture phase profile defined by a constant slope along the deflection direction, such as in (3):

$$\frac{d\varphi}{dx}(x) = -k_0 sin(\theta_{def})x + \varphi_0 \qquad (3)$$

In practice, the resulting phase distribution for any angle θ_{def} is usually wrapped to accommodate with unit-cells providing phase variation $\Delta\varphi$ of 360°. Then, it is sampled at the center location of each unit-cell to define the distribution of the phase shifts to be physically implemented. In this architecture, as in other Risley-type scanners, a deflection angle θ_{def} of 26° combined with the same output direction for the LWF is generally sufficient to achieve steering up to 60° [13]. This angle corresponds to a phase slope of 106.3° per cm at 20.2 GHz, which leads to a phase shift of 74.4° between adjacent unit-cells when considering a separation of 7 mm.

Naturally, such a phase shift cannot be nicely implemented with the limited phase range of 270° provided by the 45-mm QRSW unit-cell, as many of the required phase values would not be represented. Therefore, we selected a deflection angle close to the 26° objective but providing a sampled phase profile without any values between 270° and 360°. This was done by increasing the phase shift between adjacent unit-cells to 90°, the resulting deflection angle is therefore 32° at the center frequency of 20.2 GHz. The obtained phase distribution is therefore a strictly periodic arrangement based on a four-waveguide macro unit-cell with relative phase shifts of 0°, 90°, 180° and 270°. As a consequence, at the considered frequencies this macro unit-cell can be understood as a diffractive component with three diffractive orders among which the order +1 is favored. The macro period of 28 mm provides a deflection angle ranging from 33.9^o to 30.4^o in the 19.2-21.2 GHz band. In the following, the term grating lobes will be used to refer to the diffraction orders produced by this macro period.

The synthesis of the four phase levels is performed based on a polynomial fitting of the transmission coefficient phase extracted from the waveguide unit-cell's Floquet analysis at 20.2 GHz for normal incidence. As shown in Fig. 12, the transmitted phase is translated so that 270° corresponds with the maximum filling factor ($\tau = 1$). In this way, the synthesis will favor higher filling factors, which provide slightly better matching to free-space. Accordingly, filling factors of 0.22, 0.49, 0.67 and 1 are obtained for the phases of 0°, 90°, 180° and 270°, respectively. The synthesized four-waveguide macro unit-cell is illustrated in Fig. 13. It is worth mentioning that small circular perforations were introduced on the dielectric supporting plates to improve matching with free space. Finally, the complete phase distribution of the deflector is illustrated in Fig. 14, consisting of 772 loaded waveguides.

C. Simulation results

The functionality of the deflector was validated using CST Microwave Studio by illuminating it with a Gaussian beam with both TE and TM polarizations at normal incidence. The transmitted field patterns for both polarizations are shown at 19.2, 20.2 and 21.2 GHz in Fig. 15. The fields are normalized

ACCEPTED MANUSCRIPT / CLEAN COPY

This article has been accepted for publication in IEEE Transactions on Antennas and Propagation. This is the author's version which has not been fully edited and content may change prior to final publication. Citation information: DOI 10.1109/TAP.2024.3395908

to the broadside power of the incident Gaussian beam.

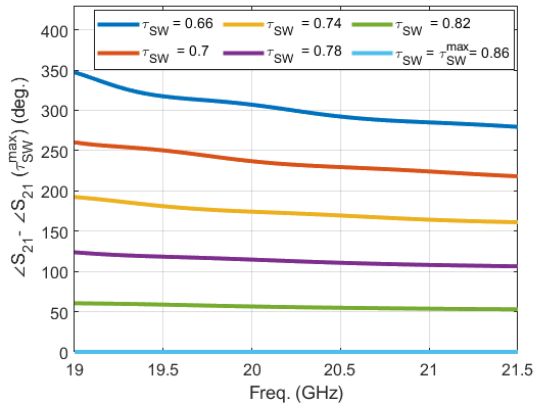

(a)

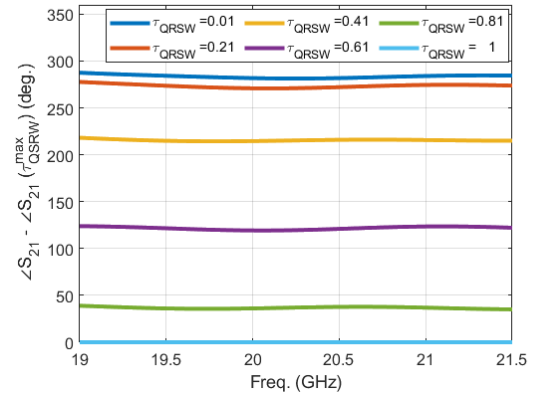

(b)

Fig. 11. Phase of S_{21} versus frequency for various filling factors obtained within a periodic environement with Floquet mode excitation : (a) SW and (b) QRSW.

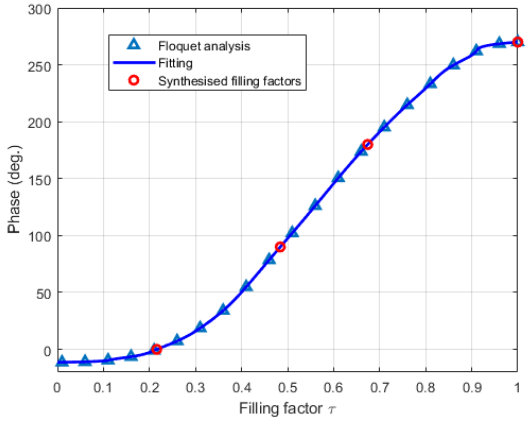

Fig. 12. Phase variation of the unit cell with respect to the filling factor to synthesize the selected four-phase-levels for the deflector function (0°, 90°, 180°, 270°).

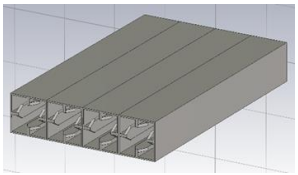

(a)

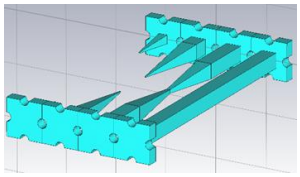

(b)

Fig. 13. Synthesized macro unit-cell. (a) Metallic waveguides. (b) Dielectric loading.

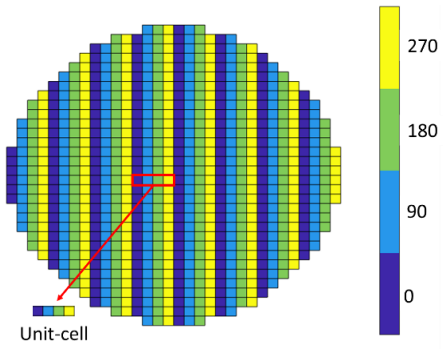

Fig. 14. Synthesized phase distribution in degrees for the deflector.

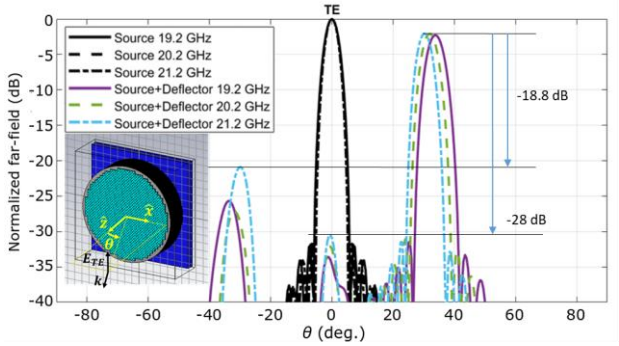

(a)

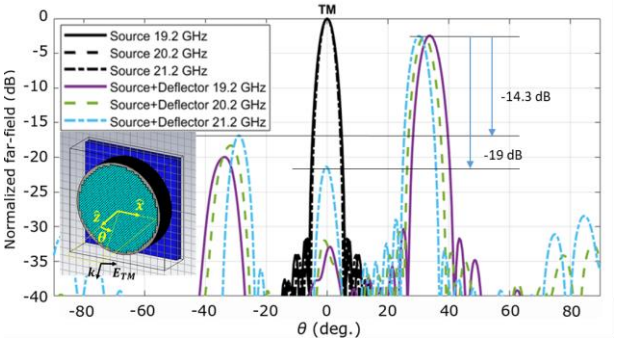

(b)

Fig. 15. Simulated transmitted field by the deflector for a normal incidence Gaussian beam. (a) TE polarization, (b) TM polarization.

The incident beam is deflected at 32° at 20.2 GHz for both polarizations. The pointing direction of the transmitted field ranges from 33.8° to 30.3° (with respect to the normal axis along $\hat{z}$) between 19.2 and 21.2 GHz. In the worst-case scenario (TM polarization), we observe relatively low grating lobes, being below -19 dB and -14.3 dB for the 0 and -1 diffraction order, respectively. The diffraction efficiencies are numerically estimated between -1.4 to -1.5 dB for TE polarization, and between -1.6 to -2 dB for TM polarization. These efficiencies include the material losses of the deflector, estimated to -0.8 to -1.1 dB for both polarizations taking into account the properties of ABS and Titanium alloy materials but neglecting the potential surface roughness of the metallic part. The metallic contribution to losses is dominant, representing about 75% of the total dissipated power, without considering surface roughness. This large contribution is related to the conductivity of the titanium alloy selected for the printing process (TA6V,

ACCEPTED MANUSCRIPT / CLEAN COPY

This article has been accepted for publication in IEEE Transactions on Antennas and Propagation. This is the author's version which has not been fully edited and content may change prior to final publication. Citation information: DOI 10.1109/TAP.2024.3395908

$\sigma = 0.6\ 10^6$ S/m), which is about 5 times lower than that of pure titanium.

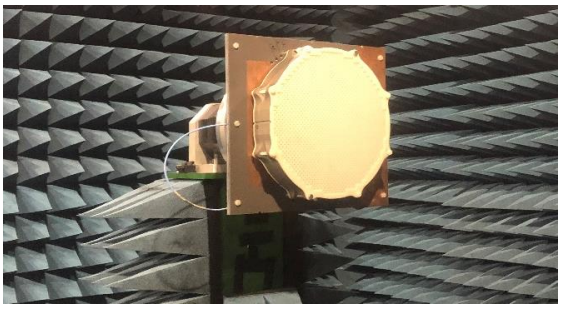

Fig. 16. Prototype mounted in the anechoic chamber during measurements.

IV. Prototyping and Measurement

The two building blocks described in the previous section have been manufactured and assembled. The spacing between the leaky-wave feed and the deflector has been numerically optimized through parametric analysis in the broadside configuration. This configuration is generally a worst-case scenario for the Risley scanner in terms of directivity and side-lobe level. It was found that a distance of 10 mm was optimal in our case. The final structure is shown in Fig. 16 while mounted in the anechoic chamber. It has a total thickness of about 62 mm. It is worth mentioning that the radiating area of the prototype corresponds to the diameter of the deflector (250 mm). The extended PCB area of the LWF is used as support to ease measurements and handling of the prototype. However, in a final version of the system such an area could be removed without affecting the performance of the antenna. A metallic support was also used to install the antenna in the anechoic chamber. The relative position of the deflector and leaky-wave feed were controlled manually. An automatic mechanical control can be considered for a more mature version of the proposed concept. In the following subsections, we describe the fabricated building blocks and provide the measurement results for the final Risley scanner for different pointing directions in the considered frequency band.

A. *Leaky-wave feed*

The prototype of the LWF, fabricated in PCB technology, is shown in Fig. 17. It has a total size of 32.6 cm× 25.5 cm × 0.315 cm. The total weight of the LWF is 0.69 kg. For fabrication purposes, the primary feed in the lower layer and the reflector are realized by metallic vias using substrate integrated waveguide (SIW) technology. Three input horns are located in the focal plane of the pillbox transition as visible in Fig. 17(b). However, during measurements, only the central horn is fed by a transition to a standard rectangular waveguide WR42 located in the back side of the supporting mechanical holders, as shown in Fig. 17(d).

B. *Deflector*

The hybrid deflector is made of a metallic array of quad-ridged dielectric loaded waveguides. The metallic part was manufactured by a conventional additive manufacturing process known as “Direct Laser Melting” (DLM). This process consists in locally and selectively melting a metallic powder bed using a directed laser beam. The procedure is repeated for each horizontal layer of the model, as is common practice for other techniques such as FDM. For this prototype, a well-known Titanium alloy (Ta6V) was chosen over aluminum alternatives for its higher melting temperature, which helps increase printing precision. It is worth mentioning that the lower thermal conductivity of Titanium can cause strong mechanical stress during manufacturing. Therefore, the final design included reinforced mounting fixtures on its external side. After printing, sandblasting was applied on the whole part to reduce the surface roughness down to about Ra = 6.5 µm. The final metallic structure is shown in Fig. 18(a), with a magnified view of the waveguide interface in Fig. 18(b). The interface photograph is taken from a slight angle, which gives the false impression of a slight bent on the ridges. Dimensional measurements at the waveguide interfaces with an optical microscope confirmed the manufacturing tolerance of ±0.1 mm.

The loading dielectric of the waveguides is made with ABS material and printed using a standard FDM technique with the Stratasys Fortus 250mc 3D-printer. To ease assembling, the dielectric loading is divided in two complementary parts, each one inserted into each side of the metallic waveguides. Special attention is given to the printing parameters, mainly the printing orientation and the layer thickness to maximize printing accuracy of the thin tips. In particular, the parts were printed vertically and the layer thickness was chosen to be 0.1778 mm, the lowest value allowed by the printer. Photographs of the dielectric parts are shown in Fig. 19 (a). One can notice the repetition of four filling ratios along one direction, as well as mounting holes on all sides.

Finally, the assembled deflector is illustrated in Fig. 19 (b). It presents a diameter of 250 mm and a thickness of 49 mm, including 45 mm for the metal waveguides and 2 mm for the dielectric loadings on each side of the deflector. The final weight of the deflector is estimated to about 3.8 kg.

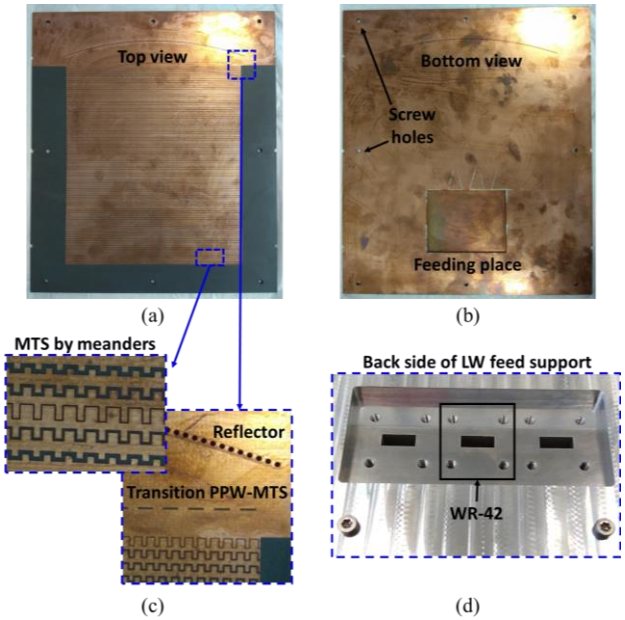

ACCEPTED MANUSCRIPT / CLEAN COPY

This article has been accepted for publication in IEEE Transactions on Antennas and Propagation. This is the author's version which has not been fully edited and content may change prior to final publication. Citation information: DOI 10.1109/TAP.2024.3395908

TABLE II
STATE-OF-THE-ART COMPARISON OF RISLEY SCANNERS WITH DISCRETE LENSES

Ref.	Design frequency f_0 (GHz)	Antenna size	Feed type	Field of view (FoW) in elevation	Peak Gain (dB)	FoW Gain variation (dB)	3-dB Gain bandwidth[2]	Polarization[3]
[11]	30	$8\lambda_0 \times 8\lambda_0 \times 10.4\lambda_0$	RLSA	39°	16.2 @ 7.5°	4	5.3%	LP
[12]	20	$\varnothing 23\lambda_0 \times 3\lambda_0$	Leaky-wave	40.6°	30.9 @ 0°	4.9	4.5%	CP
[13]	11	$6\lambda_0 \times 6\lambda_0 \times 1.3\lambda_0$	Resonant cavity	51°	19.4 @ 27°	3	N.A.	LP
[16]	21	$\varnothing 29.4\lambda_0 \times 26.6\lambda_0$	Patch	46°	35.75 @ 0°	7.5	4.8%[5]	LP
[15]	16	$\varnothing 8\lambda_0 \times 1.92\lambda_0$	Horn	52°	22.9 @ 0°	3.4	5.6%	CP
[18]	29	$\varnothing 27.1\lambda_0 \times 3.9\lambda_0$	RLSA	66°	33.1 @ 0°	5.7	6.9%	CP
[19]	10	$\varnothing 7.1\lambda_0 \times 1.1\lambda_0$	Leaky-wave	57°	22.3 @ 0°	3.5	7%	CP
This work	20.2	$\varnothing 16.8\lambda_0 \times 4.17\lambda_0$	Leaky-wave	50°	25.4 @ 0°	2.8	>10%	LP

[1]λ_0 is the free space wavelength at f_0.
[2]The relative bandwidth is derived for broadside radiation.
[3]LP and CP stand for linear and circular polarization, respectively.

Fig. 17. Prototype of the LWF. (a) Top view and (b) bottom view of the structure. (c) Details of the modulated MTS, pillbox reflector and transition pillbox-MTS. (d) Back side of the metallic holder with standard waveguides WR42 (only the central port is fed during the measurements).

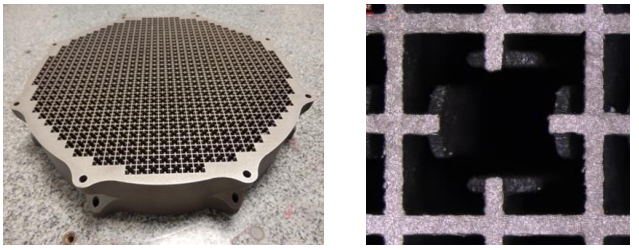

(a) (b)

Fig. 18. (a) Printed metallic waveguides of the deflector.(b) Magnified view of a waveguide unit-cell interface.

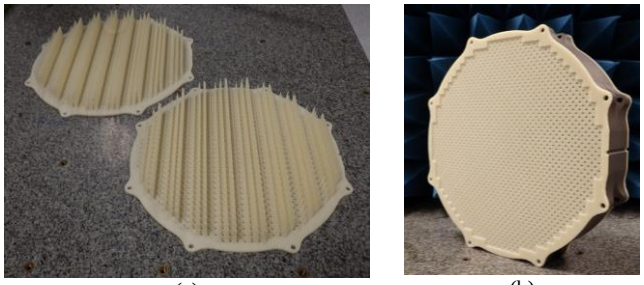

(a) (b)

Fig. 19. (a) Photograph of printed dielectric parts. (b) Assembled deflector.

C. Measurements

The Risley scanner has been measured in an anechoic chamber in the frequency band of 19.2-21.2 GHz. Three relative positions in azimuth of the deflector and the LWF were considered to illustrate the 2D-beam-steering capability of the proposed system. The measured radiation patterns are shown in Fig. 20. At the central frequency of 20.2 GHz, the SLL is lower than -12 dB for all pointing directions. A maximum gain of 25.4 dBi is measured at broadside, and varies by ±1.2 dB in the frequency band, suggesting a 3-dB gain bandwidth of at least 10%. The gain reduces to 22.6 dBi for steering at 50° in elevation. As a result of a small gap of 100 µm between the tapered transition and the lower substrate of the LWF, a significant power leakage occurred resulting in a reduced gain by about 3 to 5 dB as compared to the numerical prediction. However, a good agreement is observed between simulations and measurements in terms of pointing direction, radiated patterns, as well as SLLs although not shown here for brevity. The SLL ranges from -10.4 to -14.1 dB, except when steering at broadside at the lowest frequency of 19.2 GHz, where it reaches 9.1 dB. This SLL is comparable to the one of the LWF alone in its E-plane, as shown in Fig. 7(a), thus validating the observed results for the whole system.

The variation of the pointing direction with the frequency for the considered positions is shown in Fig. 21 and compared to full-wave results. Considering a typical beam pointing accuracy requirement of ±0.2°, the instantaneous bandwidth is estimated to be between 42 to 100 MHz for steering angles below 50°. A small discrepancy between measurements and simulations of about 2° in terms of pointing direction is visible, in particular at broadside. It was found to be related to a variation in the pointing direction of the standalone LWF.

The normalized radiation patterns along different azimuthal planes for various pointing directions are illustrated in Fig. 23. The cross-polarization components are also reported. Overall, the agreement between simulations and measurements can be considered fair, except for the maximum steering angle where the simulated main beam starts to split in a smaller side lobe. Finally, measured cross-polarization discrimination is at least 15 dB. The cross-polarization discrimination obtained in simulations does not agree with the measured one, which could be attributed to the limited simulation accuracy due to the very large computational size of the whole antenna.

Also, the input reflection coefficient is lower than -10 dB in the frequency band of interest. The radiation efficiency of the Risley scanner is numerically estimated at 20.2 GHz to about -2.7 to -3.5 dB depending on the pointing direction, including the effect of metallic surface roughness in the deflector. The LWF contributes to about 1 dB to the losses of the scanner and provides an aperture efficiency of 50%. Table II provides a comparison of the proposed solution with recent works on Risley scanners using lenses made in PCB technologies or additive manufacturing. Most advanced designs with PCB discrete lenses present a clear advantage in terms of total thickness, while the additive dielectric approach offers the

ACCEPTED MANUSCRIPT / CLEAN COPY

This article has been accepted for publication in IEEE Transactions on Antennas and Propagation. This is the author's version which has not been fully edited and content may change prior to final publication. Citation information: DOI 10.1109/TAP.2024.3395908

wider steering range with a reasonably compact size. The proposed concept exhibits an advantage in terms of 3dB-Gain bandwidth.

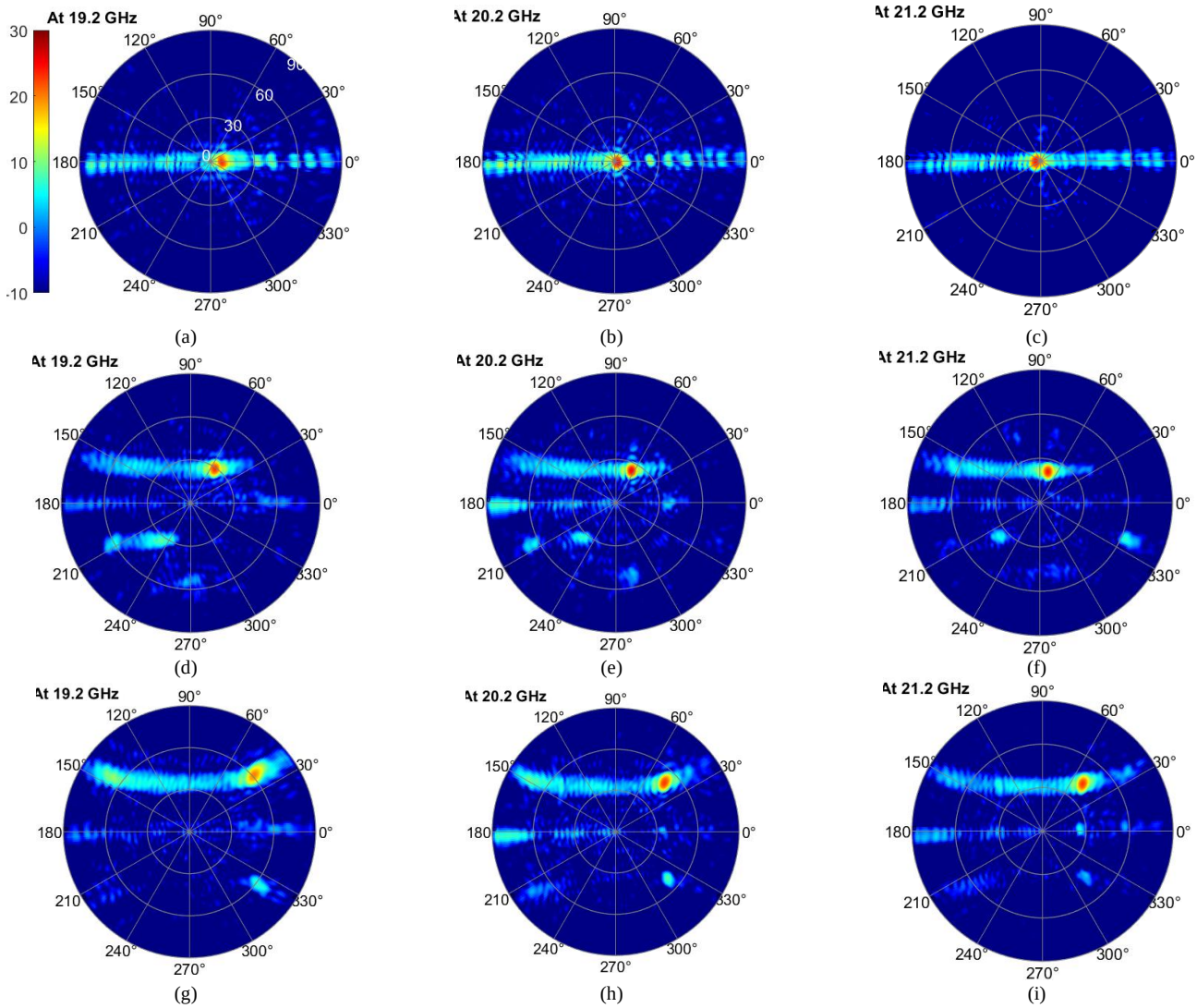

Fig. 20. Measurements of the radiated beam in the upper hemisphere in the considered frequency band of operation 19.2-21.2 GHz. (a)-(c) Nearly-broadside radiation (Ψ=180° in Fig. 2); (d)-(f) Radiation at around 25° in elevation (Ψ=135° in Fig. 2); (g)-(i) Radiation at around 50° in elevation (Ψ=90° in Fig. 2).

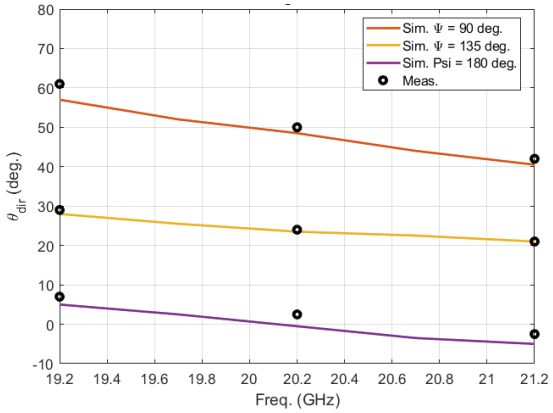

Fig. 21. Variation of the pointing direction of the Risley scanner with the frequency. Measurements are compared with full-wave numerical results.

This is the result of the design strategy to reduce dispersion in both the LWF and the deflector. The larger thickness caused by the hybrid deflector could be further reduced by using more dense dielectric materials.

V. Conclusion

We presented a Risley scanner at K band based on simplified Risley architecture consisting in a leaky-wave feed in PCB technology and a deflector made in additive manufacturing. The leaky-wave feed consists of a modulated metasurface fed by a quasi-optical system illuminating the deflector at a tilted angle of -32° in elevation, which is also the deflection angle of the deflector at 20.2 GHz

The deflector is made of two combined parts, a metallic array of quad-ridged square waveguides in titanium and a dielectric load in ABS, which were both 3D-printed. It was designed with the goal of achieving stable and efficient deflection performance within the frequency band of interest, thanks to minimized phase dispersion and limited coupling between adjacent unit-cells. Despite a gain reduction due to a misalignment of 100µm at the feeding point, measurements of the radiated field have shown the system's capability to steer

ACCEPTED MANUSCRIPT / CLEAN COPY

This article has been accepted for publication in IEEE Transactions on Antennas and Propagation. This is the author's version which has not been fully edited and content may change prior to final publication. Citation information: DOI 10.1109/TAP.2024.3395908

the main beam in 360° in azimuth and 50° in elevation with a well-formed beam, low SLL and a maximum measured gain exceeding 25 dBi. The final size of the antenna is about 250 mm in diameter with a total thickness of 62 mm. Future developments may consider the possibility to further reduce the thickness and weight of the deflector, as well as ways of improving the instantaneous bandwidth of the scanner, at the moment limited to about 80 MHz for broadside radiation.

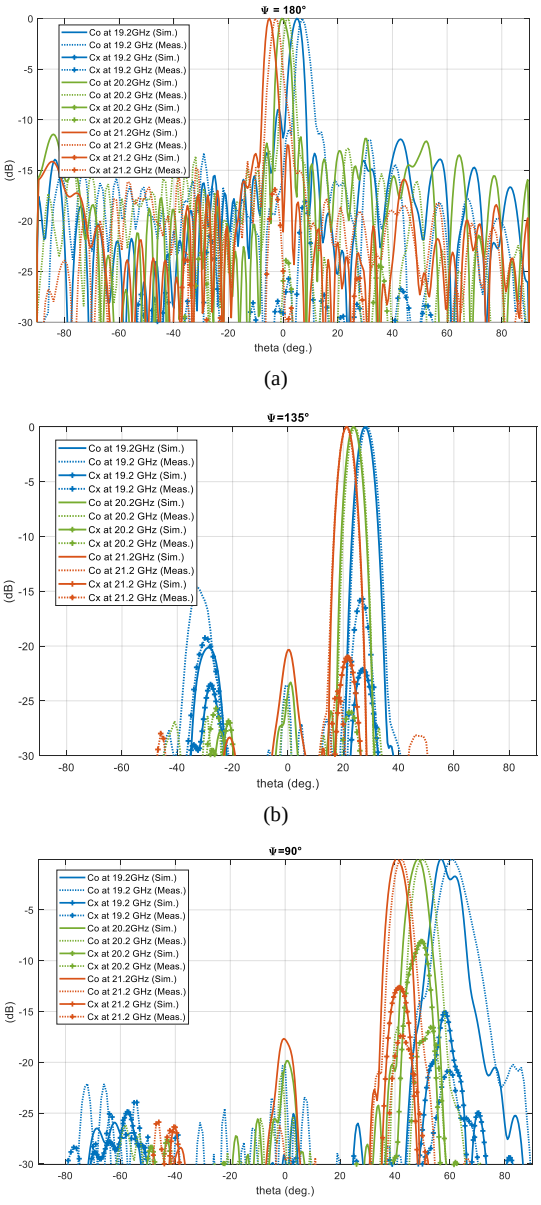

(a)

(b)

(c)

Fig. 23 Measuremed and simulated normalized raddiation patterns in the band 19.2-21.2 GHz for different relative orientations Ψ in different azimuthal cut planes. (a) Nearly-broadside radiation (Ψ=180° in Fig. 2); (b) Radiation at around 25° in elevation (Ψ=135° in Fig. 2); (c) Radiation at around 50° in elevation (Ψ=90° in Fig. 2).

ACKNOWLEDGMENT

This work was supported by the French National Research Agency (ANR) and French Ministry of Defense in the framework of the project KAPLA (ANR-17-ASTR-0010). The authors would like to thank Carole Jégou, Patrick Potier and Philippe Pouliguen for their helpful technical discussions and Laurent Cronier for developing the mechanical support used during measurements. They would also like to thank Oscar Quevedo-Teruel and his group for the first round of measurements of the prototype in KTH's facilities. This study is also supported by the European Union through the European Regional Development Fund (ERDF), and by the French region of Brittany, Ministry of Higher Education and Research, Rennes Métropole and Conseil Départemental 35, through the CPER Project SOPHIE / STIC & Ondes.

REFERENCES

[1] G. Amendola *et al*., "Low-earth orbit user segment in the Ku and Ka-band: an overview of antennas and RF front-end technologies," *IEEE Microw. Mag.*, vol. 24, no. 2, pp. 32-48, Feb. 2023.

[2] K. K. W. Low, T. Kanar, S. Zihir, and G. M. Rebeiz, "17.7–20.2-GHz 1024-element k-band SATCOM phased-array receiver with 8.1-dB/K G/T, ±70 beam scanning, and high transmit isolation," *IEEE Trans. Microw. Theory Techn.*, vol. 70, no. 3, pp. 1769–1778, Mar. 2022.

[3] K. K. W. Low, S. Zihir, T. Kanar, and G. M. Rebeiz, "A 27–31-GHz 1024-element ka-band SATCOM phased-array transmitter with 49.5-dBW peak EIRP, 1-dB AR, and ±70° beam scanning," *IEEE Trans. Microw. Theory Techn.*, vol. 70, no. 3, pp. 1757-1768, Mar. 2022.

[4] W. W. Milroy, S. B. Coppedge, and A. C. Lemons, "Variable inclination continuous transverse stub array," U.S. Patent 6 919 854 B2, Jul. 19, 2005.

[5] M. Smierzchalski, F. Foglia Manzillo, M. Del Mastro, N. Capet, B. Palacin, R. Sauleau, and M. Ettorre, "A novel dual-polarized continuous transverse stub antenna based on corrugated waveguides -part I: principle of operation and design," *IEEE Trans. Antennas Propag.*, vol. 69, no. 3, pp. 1302-1312, Mar. 2021.

[6] M. Smierzchalski, F. Foglia Manzillo, M. Del Mastro, N. Capet, B. Palacin, R. Sauleau, and M. Ettorre, "A novel dual-polarized continuous transverse stub antenna based on corrugated waveguides - part II: experimental demonstration," *IEEE Trans. Antennas Propag.*, vol. 69, no. 3, pp. 1558-2221, Mar. 2021.

[7] M. Ettorre, F. Foglia Manzillo, M. Casaletti, R. Sauleau, L. Le Coq, and N. Capet, "Continuous transverse stub array for Ka-band applications," *IEEE Trans. Antennas Propag.*, vol. 63, No. 11, pp. 4792 - 4800, Nov. 2015.

[8] R. S. Hao, Y. J. Cheng, and Y. F. Wu, "Shared-aperture variable inclination continuous transverse stub antenna working at K- and Ka-bands for mobile satellite communication," *IEEE Trans. Antennas Propag.*, vol. 68, no. 9, pp. 6656–6666, Sep. 2020.

[9] K. Singh, M. U. Afzal, M. Kovaleva, and K. P. Esselle, "Controlling the most significant grating lobes in two-dimensional beam-steering systems with phase-gradient metasurfaces," *IEEE Trans. Antennas Propag.*, vol. 68, no. 3, pp. 1389–1401, Mar. 2020.

[10] C. T. Amirault and C. A. DiMarzio, "Precision pointing using a dual wedge scanner," *Appl. Opt.*, vol. 24, no. 9, pp. 1302–1308, May 1985.

[11] H. D. Griffiths and M.R. Khan, "Antenna beam steering technique using dielectric wedges," *IEE Proc. Pt. H*, vol. 136, No. 2, Apr. 1989.

[12] M. U. Afzal, K. P. Esselle, and M. N. Y. Koli, "A beam-steering solution with highly transmitting hybrid metasurfaces and circularly polarized high-gain radial-line slot array antennas," *IEEE Trans. Antennas Propag.*, vol. 70, no. 1, pp. 365-377, Jan. 2022.

[13] F. Caminita et al., "Phase gradient metasurface for wide angle beam scanning antennas with highly reduced sidelobes," presented at the *16th Eur. Conf. Antennas Propag (EuCAP)*, Madrid, Spain, 2022.

[14] M. U. Afzal and K. P. Esselle, "Steering the beam of medium-to-high gain antennas using near-field phase transformation," *IEEE Trans. Antennas Propag.*, vol. 65, no. 4, pp. 1680–1690, Apr. 2017.

[15] H. Lei et al., "A low-profile Risley-prism-based 2-D beam-scanning circularly polarized folded transmitarray antenna at Ku-band," IEEE Trans. Antennas Propag., vol. 71, no. 7, pp. 6173–6178, July 2023.

[16] Z.-Y. Wen et al., "A dual-layer full-phase frequency-selective surface for continuous 2-D beam scanning," IEEE Trans. Antennas Propag., vol. 70, no. 11, pp. 10706–10717, Nov. 2022.

[17] M. U. Afzal, L. Matekovits, K. P. Esselle, and A. Lalbakhsh, "Beam-scanning antenna based on near-electric field phase transformation and

ACCEPTED MANUSCRIPT / CLEAN COPY

This article has been accepted for publication in IEEE Transactions on Antennas and Propagation. This is the author's version which has not been fully edited and content may change prior to final publication. Citation information: DOI 10.1109/TAP.2024.3395908

refraction of electromagnetic wave through dielectric structures," *IEEE Access*, vol. 8, pp. 199 242–199 253, 2020.
[18] T. Q. V. Hoang et al., "Low-profile highly directive 2D-beam-steering antenna in Ka-band with 3D-printed all-dielectric sub-wavelength deflectors," presented at the EuMW conference, Milan, Italy, 2022.
[19] Z. Zhang, Y. C. Zhong, H. Luyen, J. H. Booske, and N. Behdad, "A low-profile, Risley-prism-based, beam-steerable antenna employing a single flat prism," *IEEE Trans. Antennas Propag.*, vol. 70, no. 8, pp. 6646-6658, Aug. 2022.
[20] M. Bertrand et al., "Single-prism Risley scanner at Ka-band," 2023 17th European Conference on Antennas and Propagation (EuCAP), Florence, Italy, 2023, pp. 1-4.
[21] A. Oliner and A. Hessel, "Guided waves on sinusoidally-modulated reactance surfaces," *IRE Trans. Antennas Propag.*, vol. 7, no. 5, pp. 201–208, Dec. 1959.
[22] A. M. Patel and A. Grbic, "A printed leaky-wave antenna based on a sinusoidally-modulated reactance surface," *IEEE Trans. Antennas Propag.*, vol. 59, no. 6, pp. 2087-2096, Jun. 2011.
[23] J. Ruiz-García, M. Faenzi, A. Mahmoud, M. Ettorre, P. Potier, P. Pouliguen, R. Sauleau, and D. González-Ovejero, "Multi-beam modulated metasurface antenna for 5G backhaul applications at K-band," *Comptes Rendus Phys.*, vol. 22, no. S1, pp. 47-52, 2021.
[24] K. Tekkouk, M. Ettorre, E. Gandini, and R. Sauleau, "Multibeam pillbox antenna with low sidelobe level and high-beam crossover in SIW technology using the split aperture decoupling method," *IEEE Trans. Antennas Propag.*, vol. 63, no. 11, pp. 5209-5215, Nov. 2015.
[25] O. Yurduseven *et al.*, "Multibeam Si/GaAs holographic metasurface antenna at W-Band," *IEEE Trans. Antennas Propag.*, vol. 69, no. 6, pp. 3523-3528, Jun. 2021.
[26] J. Ruiz-García, M. Faenzi, A. Mahmoud *et al.*, "Quasi-optical excitation of a circularly-polarized metasurface antenna at K-band," *14th Eur. Conf. Antennas Propag. (EuCAP)*, Copenhagen, Denmark, 2020, pp. 1-4.
[27] R. Czarny *et al.*, "High permittivity, low loss, and printable thermoplastic composite material for RF and microwave applications," *IEEE Conf. Antenna Meas. Appl. (CAMA)*, 2018, pp. 1-4.
[28] M. Faenzi *et al.*, "Metasurface antennas: new models, applications and realizations," *Sci. Rep.*, vol. 9, pp. 10178, 2019.
[29] G. Minatti, D. González-Ovejero, E. Martini, and S. Maci, "Modulated metasurface antennas," in *Surface Electromagnetics: With applications in antenna, microwave, and optical engineering*, F. Yang, Y. Rahmat-Samii, Eds. Cambridge University Press, 2021.
[30] E. Martini, M. Faenzi, D. González-Ovejero, and S. Maci, "Surface-wave based metasurface antennas," in *Antenna and Array Technologies for Future Wireless Ecosystems*, Y.J. Guo and R.W. Ziolkowski, Eds., IEEE, 2022, pp.1-41.
[31] M. Bodehou, E. Martini, S. Maci, I. Huynen, and C. Craeye, "Multibeam and beam scanning with modulated metasurfaces," *IEEE Trans. Antennas Propag.*, vol. 68, no. 3, pp. 1273–1281, Mar. 2020.
[32] A. M. Patel and A. Grbic, "Effective surface impedance of a printed-circuit tensor impedance surface (PCTIS)," *IEEE Trans. Microw. Theory Techn.*, vol. 61, no. 4, pp. 1403–1413, Apr. 2013.
[33] G. Minatti, F. Caminita, E. Martini, and S. Maci, "Flat optics for leaky waves on modulated metasurfaces: Adiabatic floquet-wave analysis," *IEEE Trans. Antennas Propag.*, vol. 64, no. 9, pp. 3896–3906, Sep. 2016.

Matthieu Bertrand received the Engineering degree in electronics and signal processing from Toulouse Institute of Technology, Toulouse, France, in 2014, and the Ph.D. degree from Grenoble Alpes University, Grenoble, France, in 2017. From 2018 to 2019, he was a Post-Doctoral Researcher with the Group of Electrical Engineering (GeePs), Paris, France. During this period, he was involved in the development of fast numerical methods for substrate integrated antennas. Since 2019, he has been working on antenna research activities at Thales group Research and Technology center (TRT), Palaiseau, France.

Jorge Ruiz-García (M'23) received the M.S. degree in telecommunication engineering from the Universidad de Granada, Granada, Spain, in 2015, and the Ph.D. degree in electronics from the Université de Rennes I, Rennes, France, in 2021. Since 2022, he is a Postdoctoral Research Fellow with the Radiation Laboratory in the University of Michigan, Ann Arbor, MI, USA. He worked as an Intern at CREATIS-Lyon, Lyon, France, and in industry before joining the Institut d'Électronique et des Technologies du numéRique (IETR), Rennes, France, in 2017, to pursue his Ph.D. degree in collaboration with the Agence de l'Innovation de Défense (AID). He spent five months as a Visiting Scholar at the University of Siena, Siena, Italy, from 2019 to 2020. His research interests include metasurfaces, metamaterials, antennas, lenses, and beam-formers for microwave to submillimeter wave applications.
Dr. Ruiz-García was a recipient of the Best Paper Award in Electromagnetics at the 15th European Conference on Antennas and Propagation (EuCAP) in 2021.

Jean-François Allaeys graduated from Supelec Engineering school in 2004 (now Centrale-Supelec) and received the Ph.D. degree in physics from Paris-Sud 11 university, France, in 2007 (now Paris-Saclay University). In particular he carried his Ph.D. thesis work within Unité Mixte de Physique CNRS/Thales in Palaiseau, France (now Albert Fert Laboratory). From 2007 to 2018, he was microwave and antenna engineer at Thales Communications, Colombes (now Genevilliers), France. During this time, he worked mainly on phased array communication antennas. In 2018 and 2019 he was antenna researcher at Thales Research and Technology, Palaiseau, France, where he worked on the subject of this article. Since 2020, he has been working on radars at Thales, Limours, France.

David González Ovejero (S'01–M'13–SM'17) received the M.Sc. degree in telecommunication engineering from the Universidad Politécnica de Valencia, Valencia, Spain, in 2005, the Ph.D. degree in electrical engineering from the Université catholique de Louvain, Louvain-la-Neuve, Belgium, in 2012, and the habilitation à diriger des recherches from the Université de Rennes in 2024. From 2012 to 2014, he was a Research Associate at the University of Siena, Siena, Italy. In 2014, he joined the Jet Propulsion Laboratory, California Institute of Technology, Pasadena, CA, USA, where he was a Marie Curie Post-Doctoral Fellow. Since 2016, he has been a tenured researcher at the French National Center for Scientific Research (CNRS), Institut d'Electronique et des Technologies du numéRique (IETR), Rennes, France. His current research interests include computational electromagnetics, large phased arrays, periodic structures, metasurfaces, and submillimeter-wave antennas.

ACCEPTED MANUSCRIPT / CLEAN COPY

This article has been accepted for publication in IEEE Transactions on Antennas and Propagation. This is the author's version which has not been fully edited and content may change prior to final publication. Citation information: DOI 10.1109/TAP.2024.3395908

Dr. González Ovejero was awarded a Marie Curie International Outgoing Fellowship from the European Commission in 2013, the Sergei A. Schelkunoff Transactions Prize Paper Award from the IEEE Antennas and Propagation Society in 2016, the Best Paper Award in Antenna Design and Applications at the 11th European Conference on Antennas and Propagation in 2017, the Best Paper Award in Electromagnetics at the 15th European Conference on Antennas and Propagation in 2021, and the Best Paper Award at the International Workshop on Antenna Technology (iWAT) in 2023. Since 2019, he has served as an Associate Editor of the IEEE TRANSACTIONS ON ANTENNAS AND PROPAGATION and the IEEE TRANSACTIONS ON TERAHERTZ SCIENCE AND TECHNOLOGY.

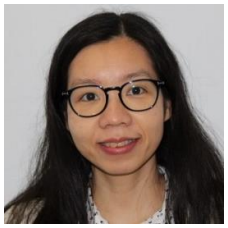

Thi Quynh Van Hoang received the Engineering degree in electronics and telecommunication from the Ho Chi Minh University of Technology, Ho Chi Minh, Vietnam, in 2007, and the M.S. and Ph.D. degrees in electronics from the University of Nice-Sophia Antipolis, Nice, France, in 2008 and 2012, respectively. After a post-doc at the Ecole Centrale de Lyon on near field coupling prediction using equivalent spherical harmonic sources, she joined Valeo (Créteil, France) in 2014 where she was mainly involved in research activities related to electromagnetic compatibility. Since 2018, she has been working at Thales Research and Technology, Palaiseau, France. Her current research interests include electromagnetic modeling, millimeter-wave beam steering antennas, periodic and non-periodic structures (absorbers, metasurfaces, and lens-based devices).

Brigitte Loiseaux graduated from Ecole Supérieur d'Optique and joined the corporate research laboratory of Thomson-CSF/LCR in 1980 (now Thales Research & Technology). There, she first worked on new concepts of color holographic optical elements for avionic display equipments. Then, after leading the activities on LCD projection, she managed the « optics and optronics » laboratory until 2008, where she worked on artificial material engineering for active radiation control. These works were carried out within collaborative projects with industrial and academic partners. In 2008, she becomes the head of the "Components and functional demonstrators" laboratory, where she initiates new research activities on new antenna concepts, building on concepts from optical architectures and the rising potential of additive manufacturing for artificial material manufacturing. Since 2021, she is senior expert within Thales group, contributing to promote the link between research activities and product development in optics and antennas. All of these experiences allowed her to contribute to more than 60 publications and 70 patents in both of these technical fields.

Ronan Sauleau (M'04–SM'06–F'18) got his postgraduate degree and M.Sc. in electrical engineering and radio communications from the Institut National des Sciences Appliquées, Rennes, France, in 1995. He received the Agrégation degree from the Ecole Normale Supérieure de Cachan, France, in 1996, and the Doctoral degree in signal processing and telecommunications and the "Habilitation à Diriger des Recherches" degree, both from the University of Rennes 1, France, in 1999 and 2005, respectively. He was an Assistant Professor and Associate Professor at the University of Rennes 1, between September 2000 and November 2005, and between December 2005 and October 2009, respectively. He has been appointed as a full Professor in the same University since November 2009.

His current research fields are numerical modeling, millimeter-wave beam steering antennas, substrate integrated waveguide antennas, lens-based focusing devices, periodic and non-periodic structures (FSS, metasurfaces, polarizers, reflectarrays, and transmitarrays) and biological effects of millimeter waves. He has been involved in more than 80 research projects at the national and European levels and has co-supervised 29 post-doctoral fellows, 63 PhD students and 50 master students. He has received 25 patents and is the author or coauthor of 300 journal papers and more than 600 publications in international conferences and workshops. He was co-director of the research Department 'Antenna and Microwave Devices' at IETR and deputy director of IETR between 2012 and 2016. He is now director of IETR. Prof. Sauleau received the 2004 ISAP Conference Young Researcher Scientist Fellowship (Japan) and the first Young Researcher Prize in Brittany, France, in 2001 for his research work on gain-enhanced Fabry-Perot antennas. In September 2007, he was elevated to Junior member of the "Institut Universitaire de France". He was awarded the Bronze medal by CNRS in 2008, and the silver medal in 2020. He received the 2021 Antenna EurAAP Award. He was the co-recipient of several international conference awards with some of his students (Int. Sch. of BioEM 2005, BEMS'2006, MRRS'2008, E-MRS'2011, BEMS'2011, IMS'2012, Antem'2012, BioEM'2015, EuCAP'2019, EuCAP'2021, EuMW'2022). He served as a guest editor for the IEEE Antennas Propogat. Special Issue on "Antennas and Propagation at mm and sub mm waves". He served as a national delegate for several EU COST actions. He has served as a national delegate for EurAAP and as a member of the board of Director of EurAAP from 2013 to 2018.

Romain Czarny graduated from Ecole Nationale Supérieure des Télécommunications (ENST, now Telecom Paris), Paris, France, in 2002. He received his Ph.D. degree in electronics in 2006 from Lille 1 university, Lille, France, working on optically driven sub-millimeters sources in collaboration with Thales Research & Technology, Palaiseau, France, and the Institut d'Electronique, de Microélectronique et de Nanotechnologie (IEMN). After a 3-year period working on ns laser sources in Thales Laser (now Thales LAS), he joined

ACCEPTED MANUSCRIPT / CLEAN COPY

This article has been accepted for publication in IEEE Transactions on Antennas and Propagation. This is the author's version which has not been fully edited and content may change prior to final publication. Citation information: DOI 10.1109/TAP.2024.3395908

TRT between 2009 and 2017 as head of the "new antenna concepts" research activities. During this period he worked on the subject of this article. Since 2017 he is with Thales DMS France where his activities are dedicated to AESA airborne antenna development.

Mauro Ettorre (M'08–SM'15-F'23) received a Laurea degree "summa cum laude" in Electrical Engineering, and a Ph.D. degree in Electromagnetics from the University of Siena, Italy, in 2004 and 2008, respectively. Part of his Ph.D. work was developed at the Netherlands Organisation for Applied Scientific Research (TNO), The Hague, the Netherlands, where he later worked as an Antenna Researcher. Since 2023, he is a Professor at Michigan State University, East Lansing, USA. Previously, he was a Research Scientist at the Centre National de la Recherche Scientifique (CNRS), IETR laboratory, France. From 2008 to 2010, Dr. Ettorre was a Postdoctoral Fellow at IETR, University of Rennes 1, France. In 2010 and 2016, he was a Visiting Scholar in the Department of Electrical Engineering and Computer Science, University of Michigan, USA. From 2014 until 2020, he co-led the multi-beam antenna activity for satellite applications in the joint laboratory between IETR and Thales Alenia Space, France. From 2016 until 2021, he was member of the French National Committee for Scientific Research, CNRS, France.

Dr. Ettorre's research interests include the analysis and design of quasi-optical systems, periodic structures, wideband arrays, millimeter-wave antennas, non-diffractive radiation and localized waves. Since 2017 and 2023, he serves as Associate Editor and Track Editor for the IEEE Transaction on Antennas and Propagation, respectively. In 2017, 2018, and 2019 he was member of the best paper award selection committee for the IEEE Transactions on Terahertz Science and Technology. In 2020 and 2021 he was appointed EurAAP (European Association on Antennas and Propagation) ambassador. Since 2021, he is member of the technical committee MTT-29 Microwave Aerospace Systems. Since 2023, he is member of the Board of Directors of EurAAP.

The research activities of Dr. Ettorre have been recognized with several prizes, including the Innovation Award at the 2018 ESA Antenna Workshop in the Netherlands, the Best Paper Award in Electromagnetics and Antenna Theory at the 2018 European Conference on Antennas and Propagation (EuCAP), London, UK, the Best Antennas Paper Award at EuCAP 2021, Düsseldorf, Germany and Best Paper Award at the 2023 International Workshop on Antenna Technology (iWAT), Aalborg, Denmark.

ACCEPTED MANUSCRIPT / CLEAN COPY